INTERNATIONAL JOURNAL FOR NUMERICAL METHODS IN ENGINEERING
Int. J. Numer. Meth. Engng 2009; **77**:214–239
Published online 22 July 2008 in Wiley InterScience (www.interscience.wiley.com). DOI: 10.1002/nme.2411

The extended finite element method for fracture in composite materials

D. B. P. Huynh[‡] and T. Belytschko[*, †]

Department of Mechanical Engineering, Northwestern University, Evanston, IL 60208, U.S.A

SUMMARY

Methods for treating fracture in composite material by the extended finite element method with meshes that are independent of matrix/fiber interfaces and crack morphology are described. All discontinuities and near-tip enrichments are modeled using the framework of local partition of unity. Level sets are used to describe the geometry of the interfaces and cracks so that no explicit representation of either the cracks or the material interfaces are needed. Both full 12 function enrichments and approximate enrichments for bimaterial crack tips are employed. A technique to correct the approximation in blending elements is used to improve the accuracy. Several numerical results for both two-dimensional and three-dimensional examples illustrate the versatility of the technique. The results clearly demonstrate that interface enrichment is sufficient to model the correct mechanics of an interface crack. Copyright © 2008 John Wiley & Sons, Ltd.

Received 5 May 2008; Accepted 13 May 2008

KEY WORDS: extended finite elements method; bimaterial; composite

1. INTRODUCTION

The fracture analysis of composites by standard finite element method (FEM) techniques is a formidable task. Even aligning a mesh so that the fiber/matrix interfaces correspond to element interfaces, which is necessary in standard FEM, is quite difficult for complex composites. The additional challenge of conforming the crack surfaces to elements complicates the task further.

In this article, a general methodology is described whereby neither the fiber/matrix interfaces nor the crack surfaces need to conform to the mesh for obtaining stress intensity factors (SIFs) in

[*]Correspondence to: T. Belytschko, Department of Mechanical Engineering, Northwestern University, Evanston, IL 60208, U.S.A.
[†]E-mail: tedbelytschko@northwestern.edu
[‡]Post-Doctoral Research Fellow, Department of Mechanical Engineering.

composites at interfaces. In other words, the alignment of these features can be entirely arbitrary with respect to the mesh. The method is based on the extended FEM (XFEM) [1, 2], a well-known method that improves the versatility of standard finite element (FE) approximations using the partition of unity concept [3] to incorporate *a priori* knowledge of the solution into the approximation space [4, 5]. Perhaps the most important advantage of XFEM is that it can model discontinuities without the need to conform the mesh with the discontinuities [6]. The method is also able to improve the approximated solution around singular features such as crack tips, notches or corners by proper corrections (or enrichments) and thus is a flexible and powerful tool in the field of fracture mechanics. For example, the method was employed to analyze and simulate two-dimensional [7–9] and three-dimensional [10–12] elastic crack growth. We might add that XFEM has a wide variety of applications, such as dynamic crack propagation [13, 14], dislocations [15, 16] and large strain fracture mechanics [17]. XFEM also shares some features with the s-method of Fish [18] and Fish and Markofelas [19]. A recent application of the s-method to material failure is given in [20].

XFEM is based on a local partition of unity that entails the blending between enriched and unenriched elements. Although this causes no problems for strong discontinuities, for the weak discontinuities at material interfaces and for crack tip enrichments, it requires blending that degrades accuracy slightly [21, 22]. A great deal of study has been devoted to improving the accuracy of XFEM by correcting the approximation in such blending elements. For example, the approximation is corrected by an assumed strain field by Chessa *et al*. [21] and by a discontinuous Galerkin approach by Gracie *et al*. [23]. Fries [24] and Gracie *et al*. [23] have developed a simple approach to neutralize the effect of the parasitic terms by using a ramp function that smoothly eliminates the unwanted terms in blending elements. It should be pointed out that this is only necessary for low-order elements, as noted in [21].

The methods for applying XFEM to the analysis of fracture in composite or layered structures are still nascent. Sukumar *et al*. [25], Liu *et al*. [26] and Nagashima *et al*. [27] apply XFEM to solve two-dimensional bimaterial interfacial crack problems. However, these authors employed only crack tip enrichments and the computational meshes were aligned with the material interfaces. Recently, Hettich *et al*. [28] apply XFEM to model failure in material interfaces in two-dimensional problems.

In this article, we develop a method to solve both two-dimensional and three-dimensional composites with cracks. Both material interfaces and singularities are modeled by XFEM, and no mesh restriction is imposed. Consequently, the meshing of composites is simplified immensely. It is possible to use structured (i.e. Cartesian) meshes or unstructured meshes that do not conform to the interfaces or to the crack surfaces but are generated to account only for the outside surfaces of the model. Standard FEM methods require that element edges coincide with the material interfaces and with crack surfaces. The benefits of removing this requirement are that they tremendously facilitate the analysis of composites. The methodology is described for isotropic materials with interfaces; hence, it is only applicable to models with isotropic fibers and matrix materials.

This article is organized as follows. In the following section, we shall briefly review the standard XFEM and the corrected XFEM by Fries [24]. In Section 3, we describe the method to extract the SIFs for both two-dimensional and three-dimensional cases using the interaction integral idea [29]. In Section 4, we present numerical results for several example problems. Finally, in Section 5, we draw conclusions and discuss directions for future works.

DOI: 10.1002/nme

2. XFEM

In this section, we shall review our level set description of interfaces and cracks and the standard XFEM; we then present the corrected XFEM using corrections in blending elements. We begin with a review of the level set descriptions.

2.1. Level set descriptions

The methods developed in this article employ level sets, i.e. implicit surfaces, although these are not an essential part of the formulation and alternative methods for describing the crack surfaces and material interfaces can be used. However, level set methods provide a concise means for describing the enrichments and become very useful for evolving cracks. Level set methods for interface modeling and crack modeling were introduced in Belytschko *et al*. [30], Sukumar *et al*. [31] and Stolarska *et al*. [32], and also studied by Duflot [33].

The matrix/fiber interfaces are represented by the zero level set surfaces $f_\alpha^{\text{int}}(\mathbf{x})$ through

$$f_\alpha^{\text{int}}(\mathbf{x})=0, \quad \alpha=1\ldots n_{\text{int}} \tag{1}$$

where n_{int} is the number of interfaces. For simplicity, we assume here that the zero level set surfaces are non-intersecting.

To represent cracks, a set of similar level set functions is introduced,

$$f_\alpha^{\text{cr}}(\mathbf{x})=0, \quad \alpha=1\ldots n_{\text{cr}} \tag{2}$$

for which the zero level set gives the crack surface. For the purpose of defining the crack tips/fronts, another set of level sets, $g_\alpha^{\text{cr}}(\mathbf{x})$, $\alpha=1,\ldots,n_{\text{cr}}$, is defined such that the crack α is given by

$$\mathbf{x}\ni f_\alpha^{\text{cr}}(\mathbf{x})=0 \quad \text{and} \quad g_\alpha^{\text{cr}}(\mathbf{x})\geqslant 0 \tag{3}$$

and the crack tips/fronts of crack α are given by

$$\mathbf{x}\ni f_\alpha^{\text{cr}}(\mathbf{x})=0 \quad \text{and} \quad g_\alpha^{\text{cr}}(\mathbf{x})=0 \tag{4}$$

as shown in Figure 1.

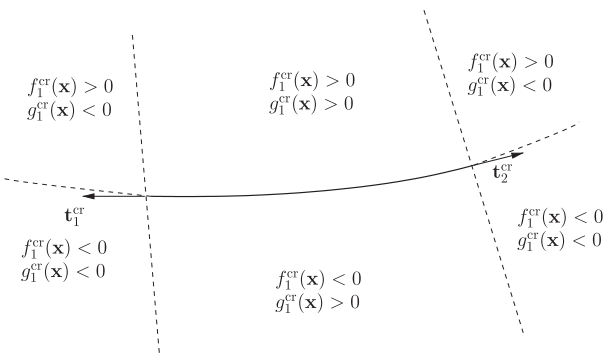

Figure 1. Level set description for a two-dimensional crack.

DOI: 10.1002/nme

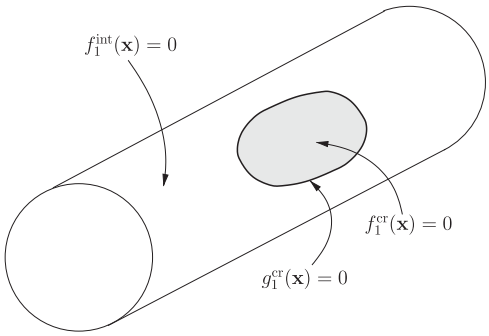

Figure 2. The level set descriptions for an interfacial crack.

We note that, for the case of more than one crack tip/front associated with the same crack α, the function $g_\alpha^{\text{cr}}(\mathbf{x})$ for the crack α is chosen as

$$g_\alpha^{\text{cr}}(\mathbf{x}) = \max_i g_{\alpha,i}^{\text{cr}}(\mathbf{x}) \tag{5}$$

where $g_{\alpha,i}^{\text{cr}}(\mathbf{x})$ denotes the level set associated with the ith tip/front of crack α. When the crack surface α lies on an interface β, $f_\alpha^{\text{cr}}(\mathbf{x}) = f_\beta^{\text{int}}(\mathbf{x})$, as shown in Figure 2.

2.2. *Preliminaries*

In this section we shall review some fundamental definitions and standard results of mechanics and FEs. Let us denote $\mathbf{u}$ as the displacement and $\varepsilon(\mathbf{u})$ as the strain corresponding to $\mathbf{u}$, the weak form of the equilibrium equation for a domain $\Omega \in \mathbb{R}^n$, where $n = 1, \ldots, 3$ is the dimension of the problem, which reads for $\mathbf{u} \in \mathscr{U}$, as

$$\int_\Omega \boldsymbol{\varepsilon}(\mathbf{u}) : \mathbf{C} : \boldsymbol{\varepsilon}(\mathbf{v})\, \mathrm{d}\Omega = \int_\Omega \mathbf{b} \cdot \mathbf{v}\, \mathrm{d}\Omega + \int_{\Gamma_t} \boldsymbol{\sigma}_0 \cdot \mathbf{v}\, \mathrm{d}\Gamma_N \quad \forall \mathbf{v} \in \mathscr{U}_0 \tag{6}$$

where $\mathbf{b}$ is the body force, $\boldsymbol{\sigma}_0$ is the traction applied on Γ_N and $\mathbf{C}$ is the elasticity tensor. The admissible Hilbert spaces $\mathscr{U}$ and $\mathscr{U}_0$ are defined by

$$\mathscr{U} = \{\mathbf{v} \in (H^1(\Omega))^n \,|\, \mathbf{v} = \mathbf{v}_0 \text{ on } \Gamma_D\}, \quad \mathscr{U}_0 = \mathscr{U}(\mathbf{v}_0 = 0) \tag{7}$$

where $\mathbf{v}_0$ is the prescribed displacement of Γ_D. We discretize the domain Ω into N_{el} elements, which is formed by the nodal set S_N of size N. We shall need a nodal subset S_D of S_N ($S_D \subset S_N$), which we shall call our 'enrichment' nodal set. The enrichment nodal set contains the nodes of the elements, which are crossed by the surface on which $\mathbf{u}$ is discontinuous, and the subdomains in which the approximated $\mathbf{u}$ field is 'enhanced' by 'enrichments,' such as regions near crack tips, etc.

In the following sections, for the sake of simplicity, we only consider one enrichment in the approximation. The extension to multiple enrichments is very simple and straightforward [1, 24].

DOI: 10.1002/nme

2.3. Extended FE approximation

We use the blending of Fries [24] (also see Gracie *et al*. [23]) with the shifting proposed in Belytschko *et al*. [6]. The standard XFEM approximation [1] is

$$\mathbf{u}(\mathbf{x}) = \sum_{i=1}^{N_{\text{el}}} \mathbf{u}_i \phi_i(\mathbf{x}) + \sum_{i \in S_D} a_i \phi_i^*(\mathbf{x}) \psi_i(\mathbf{x}) \tag{8}$$

where $\phi_i(\mathbf{x})$, $\mathbf{u}_i(\mathbf{x})$, $\psi_i(\mathbf{x})$ are the standard FE shape functions, the unknowns (displacement), and the local enrichment function of node i, respectively, where S_D is the set of enrichment nodes. The functions $\phi_i^*(\mathbf{x})$ are also a set of FE shape functions, although not necessarily the same as $\phi_i(\mathbf{x})$; they also form a partition of unity,

$$\sum_{i \in S_D} \phi_i^*(\mathbf{x}) = 1 \tag{9}$$

We can then recognize that in some elements, such as those elements not completely defined by nodes in S_D, $\phi(\mathbf{x})$ does not build a partition of unity; thus the global enrichment function $\psi_i(\mathbf{x})$ cannot be represented exactly in such elements. We shall correct the approximation in those elements using the corrected XFEM [23, 24]. For the sake of convenience, we shall call the elements with nodes only in S_D *local enrichment elements* and elements with some nodes in S_D *blending elements*.

We first define a nodal subset S_A, consisting of all element nodes of the local enrichment elements and blending elements. We then recognize that $S_D \subset S_A$, as shown in Figure 3. Following the procedure described in [24], we define our XFEM approximation as

$$\mathbf{u}(\mathbf{x}) = \sum_{i=1}^{N_{\text{el}}} \mathbf{u}_i \phi_i(\mathbf{x}) + \sum_{i \in S_A} a_i \phi_i^*(\mathbf{x}) R(\mathbf{x}) \psi_i^s(\mathbf{x}) \tag{10}$$

where

$$R(\mathbf{x}) = \sum_{i \in S_A} \phi_i^*(\mathbf{x}) \tag{11}$$

is a ramp function defined upon the partition of unity shape function $\psi_i^*(\mathbf{x})$; and $\psi_i^s(\mathbf{x})$ are the shifted enrichment functions defined by

$$\psi_i^s(\mathbf{x}) = \psi_i(\mathbf{x}) - \psi_i(\mathbf{x}_i) \quad \forall i \in S_A \tag{12}$$

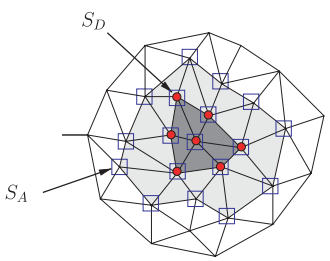

Figure 3. The enrichment nodal set S_D (•) and S_A (□).

DOI: 10.1002/nme

It is noted that the ramp function $R(\mathbf{x})$ is unity in enriched elements, whereas it varies from unity to zero in the blending elements.

We stop here to make several observations.

- With the introduction of the ramp function, the modified enrichment functions $\psi_i^s(\mathbf{x})$ vary continuously from the original enrichment functions $\psi_i(\mathbf{x})$ to zero in the blending elements. Furthermore, $\psi_i^s(\mathbf{x}) \equiv \psi_i^s(\mathbf{x})$ in local enrichment elements; and $\psi_i^s(\mathbf{x}) = 0$ in the standard non-enriched elements, which include elements that are formed partly by nodes in S_A. As a result, there are no unwanted terms (second terms in (8)) in the blending elements that leads to a better accuracy. As shown in [24], optimal convergence rates are recovered.
- $\phi_i^*(\mathbf{x})$ is a partition of unity in both the local enrichment elements and blending elements. Thus, the approximation is capable of representing the enrichment functions $\psi_i(\mathbf{x})$ exactly in the local enrichment elements and standard unenriched elements, while representing the same enrichment functions smoothly in the blending elements.

2.4. Enrichment functions

2.4.1. Weak discontinuities. Weak discontinuities are discontinuities in the derivatives of the approximation. This class of discontinuity occurs when the coefficients of the corresponding partial different of equations are discontinuous, such as interfaces between materials or between phases of materials. The enrichment for these discontinuities is the so-called 'abs-enrichment'

$$\psi_\alpha(\mathbf{x}) = |f_\alpha^{\text{int}}(\mathbf{x})| \tag{13}$$

where $f_\alpha^{\text{int}}(\mathbf{x})$ is the level set associated with interface α and is chosen as a signed distance function [6].

2.4.2. Strong discontinuities. Strong discontinuities are discontinuities in the approximation, which are used to model cracks. For this class of discontinuities, the Heaviside function is used for the enrichment function,

$$\psi_\alpha(\mathbf{x}) = H(f_\alpha^{\text{cr}}(\mathbf{x}) g_\alpha^{\text{cr}}(\mathbf{x})) \tag{14}$$

where $f_\alpha^{\text{cr}}(\mathbf{x})$ and $g_\alpha^{\text{cr}}(\mathbf{x})$ are the level sets that define the crack surface α. We note that for this enrichment, blending elements are no longer necessary if the order of the partition of unity functions $\phi_i^*(\mathbf{x})$ are the same as or lower than that of the usual standard FE shape functions $\phi_i(\mathbf{x})$. Furthermore, the shifting operation (12) automatically reduces the enrichment function in the blending elements to zero [24].

2.4.3. Crack tip enrichments. It is well known that stresses and strains are singular at crack tips in elastic materials. The crack tip enrichments in XFEM are chosen to be the asymptotic functions or leading terms of the analytical displacement fields. Here we consider the crack tip solutions for a crack coincident with the interface between two isotropic materials. These are given in the Appendix. We list here several crack tip enrichment functions for some common cases. In all of the functions below, r and θ correspond to a local polar coordinate system defined by the geometry

DOI: 10.1002/nme

at the crack tip, but to render these enrichments applicable to curved surfaces we express these variables in terms of the level set functions of the crack α by

$$r = \sqrt{(f_\alpha^{\mathrm{cr}}(\mathbf{x}))^2 + (g_\alpha^{\mathrm{cr}}(\mathbf{x}))^2}$$
$$\theta = \tan^{-1} \frac{f_\alpha^{\mathrm{cr}}(\mathbf{x})}{g_\alpha^{\mathrm{cr}}(\mathbf{x})} \tag{15}$$

(We omit the subscript α on r and θ). Note that in two dimensions, the sign of θ must be reversed at the second (right) tip of the crack to be consistent with the local polar coordinate system.

For a two-dimensional crack aligned to the interface of a material interface, the following 12 enrichments are used:

$$\begin{aligned}[\psi_{\alpha,j}(\mathbf{x})(r,\theta), j=1\ldots12] \equiv \Bigg\{ & \sqrt{r}\cos(\varepsilon\log r)\,\mathrm{e}^{-\varepsilon\theta}\sin\frac{\theta}{2}, \sqrt{r}\cos(\varepsilon\log r)\,\mathrm{e}^{\varepsilon\theta}\sin\frac{\theta}{2}\sin\theta, \\ & \sqrt{r}\cos(\varepsilon\log r)\,\mathrm{e}^{-\varepsilon\theta}\cos\frac{\theta}{2}, \sqrt{r}\cos(\varepsilon\log r)\,\mathrm{e}^{\varepsilon\theta}\cos\frac{\theta}{2}\sin\theta, \\ & \sqrt{r}\cos(\varepsilon\log r)\,\mathrm{e}^{\varepsilon\theta}\sin\frac{\theta}{2}, \sqrt{r}\sin(\varepsilon\log r)\,\mathrm{e}^{\varepsilon\theta}\sin\frac{\theta}{2}\sin\theta, \\ & \sqrt{r}\cos(\varepsilon\log r)\,\mathrm{e}^{\varepsilon\theta}\cos\frac{\theta}{2}, \sqrt{r}\sin(\varepsilon\log r)\,\mathrm{e}^{\varepsilon\theta}\cos\frac{\theta}{2}\sin\theta, \\ & \sqrt{r}\sin(\varepsilon\log r)\,\mathrm{e}^{-\varepsilon\theta}\sin\frac{\theta}{2}, \sqrt{r}\sin(\varepsilon\log r)\,\mathrm{e}^{-\varepsilon\theta}\sin\frac{\theta}{2}\sin\theta, \\ & \sqrt{r}\sin(\varepsilon\log r)\,\mathrm{e}^{\varepsilon\theta}\sin\frac{\theta}{2}, \sqrt{r}\sin(\varepsilon\log r)\,\mathrm{e}^{\varepsilon\theta}\sin\frac{\theta}{2}\sin\theta \Bigg\} \end{aligned} \tag{16}$$

where ε is the bimaterial constant that depends on the two material properties and is given in the Appendix.

In the three-dimensional case, an additional enrichment,

$$\psi_{\alpha,13}(r,\theta) = \sqrt{r}\sin\frac{\theta}{2} \tag{17}$$

is used in conjunction with the above 12 enrichments.

For a crack that is not coincident with an interface in two-dimensional and three-dimensional homogeneous elastic materials, the following four enrichments given by Flemming *et al.* [34] in the context of meshless methods are used:

$$[\psi_{\alpha,j}(r,\theta), j=1\ldots4] \equiv \left\{ \sqrt{r}\sin\frac{\theta}{2}, \sqrt{r}\sin\frac{\theta}{2}\sin\theta, \sqrt{r}\cos\frac{\theta}{2}, \sqrt{r}\cos\frac{\theta}{2}\sin\theta \right\} \tag{18}$$

These four enrichment functions are recovered from the thirteen enrichment functions for the case $\varepsilon = 0$.

We note that the enrichment functions are constructed from the analytical solution of straight/flat interfacial cracks. However, our results show that they can also be used for curved/non-planar interfacial cracks, assuming that in the vicinity of the crack front, the crack lines are assumed

DOI: 10.1002/nme

to be straight/flat as the element size decreases. It has previously been shown that sufficient mesh refinement usually provides accurate results for curved crack fronts [11, 35].

2.5. Implementation

Special integration schemes are needed for enriched elements when elements are cut by discontinuities. For those elements, the 'subdivision' integration strategy is used [9]. The element is first subdivided into several sub-elements (triangles in two dimensions and tetrahedra in three dimensions), such that the edges or faces of these sub-elements are aligned with the discontinuities. A high-order Gaussian integration scheme is then employed for each of these sub-elements. For blending elements, since there is no 'cut,' a high-order Gaussian integration scheme usually suffices. We use a seventh-order Gaussian integration scheme for each of these sub-elements and a ninth-order Gaussian integration scheme in blending elements. The derivatives of the enrichment functions are calculated using a finite difference scheme.

The introduction of more enrichment nodes in the XFEM formulation impairs the conditioning of the stiffness equations slightly. In fact, it has been shown that several degrees of freedom have to be eliminated in order to make the linear system non-singular [24]. Hence, the Gaussian elimination solver is not able to provide good accuracy; we solve the system by the conjugate gradient iterative algorithm.

3. SIF CALCULATION

3.1. Two-dimensional SIF of bimaterial cracks

We define a local coordinate system $(\mathbf{e}_1, \mathbf{e}_2)$ associated with the crack tip as shown in Figure 4. The (path-independent) contour J-integral is defined as

$$I = \int_{\Gamma_A} P_{1j} n_j \, \mathrm{d}\Gamma_A \tag{19}$$

where $P_{1j} = \frac{1}{2}\sigma_{ik}\varepsilon_{ik} - \sigma_{ij}u_{i,1}$, Γ_A is an arbitrary path around the crack tip and $\mathbf{n}$ denotes the outward normal vector of a point on Γ_A. It is well known that the J-integral is path-independent for cracks in homogeneous material. For a crack in inhomogeneous material, it has been proven that for a crack on the interface, the J-integral remains globally path-independent [36]. We may therefore use the J-integral for the extraction of mixed-mode SIFs.

Next, we define the contour interaction integral [7]

$$I = \int_{\Gamma_A} P_{1j}^{\mathrm{aux}} n_j \, \mathrm{d}\Gamma_A \tag{20}$$

where $P_{1j}^{\mathrm{aux}} = \sigma_{ik}\varepsilon_{ik}^{\mathrm{aux}} - \sigma_{ij}u_{i,1}^{\mathrm{aux}} - \sigma_{ij}^{\mathrm{aux}}u_{i,1}$, and u_i^{aux}, $\varepsilon_{ij}^{\mathrm{aux}}$ and $\sigma_{ij}^{\mathrm{aux}}$ are the auxiliary displacement, strain and stress fields, respectively. The interaction integral is related to the SIFs K_1 and K_2 through the relation

$$I = \frac{2}{E^* \cosh^2(\pi\varepsilon)}[K_1 K_1^{\mathrm{aux}} + K_2 K_2^{\mathrm{aux}}] \tag{21}$$

DOI: 10.1002/nme

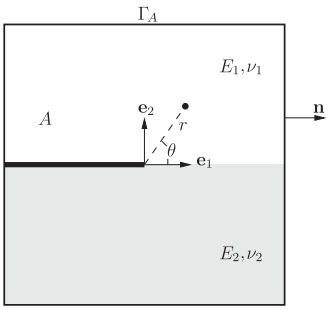

Figure 4. The two-dimensional computational domain.

where K_1^{aux} and K_2^{aux} are local auxiliary SIFs for the auxiliary field and E^* is the effective Young's modulus given by

$$E^* = \frac{2E_1' E_2'}{E_1' + E_2'} \quad \text{where } E' = \begin{cases} \dfrac{E}{1-\nu^2} & \text{plane strain} \\ E & \text{plane stress} \end{cases} \tag{22}$$

The SIFs K_1 and K_2 can now be computed using a proper choice of K_1^{aux} and K_2^{aux}. For example, by selecting $K_1^{\text{aux}} = 1$ and $K_2^{\text{aux}} = 0$ and evaluating $I_1 \equiv I(K_1^{\text{aux}} = 1, K_2^{\text{aux}} = 0)$, we can evaluate K_1 by

$$K_1 = \frac{E^* \cosh^2(\pi\varepsilon)}{2} I_1 \tag{23}$$

In practice, we evaluate the contour interaction integral using its domain form,

$$I = -\int_A P_{1j}^{\text{aux}} q_{,j} \, \mathrm{d}A \tag{24}$$

where q is an arbitrary smooth weighting function that is unity at the crack tip and zero on the outer contour Γ_A, and A is a close domain defined on the contour Γ_A. The auxiliary fields are chosen as the asymptotic terms of the crack tip fields as listed in the Appendix.

3.2. Three-dimensional SIF of bimaterial cracks

For the point p located on the crack front, we first define a domain V surrounding the point p. The domain V intercepts the arc L_c of the crack front as shown in Figure 5. We next associate a local basis $(\mathbf{e}_1, \mathbf{e}_2, \mathbf{e}_3)$ with any point inside the domain V and define a sufficiently smooth test function $\mathbf{q} = \alpha_q(\mathbf{x})\mathbf{e}_1$ that is at a tangent to the crack faces on the crack and on the front. Here, the scalar function $\alpha_q(\mathbf{x})$ is a continuous function that is unity at p and vanishes on the boundary of V. The basis vectors $(\mathbf{e}_1, \mathbf{e}_2, \mathbf{e}_3)$ at a point $\mathbf{x}$ in the global cartesian coordinate system are defined based on the level set functions $f_\alpha^{\text{cr}}(\mathbf{x})$ and $g_\alpha^{\text{cr}}(\mathbf{x})$ by

$$\mathbf{e}_1 = \sum_{i \in N_e} \phi_i(\mathbf{x}) \nabla g_\alpha^{\text{cr}}(\mathbf{x}_i), \quad \mathbf{e}_2 = \sum_{i \in N_e} \phi_i(\mathbf{x}) \nabla f_\alpha^{\text{cr}}(\mathbf{x}_i), \quad \mathbf{e}_3 = \mathbf{e}_1 \times \mathbf{e}_2 \tag{25}$$

DOI: 10.1002/nme

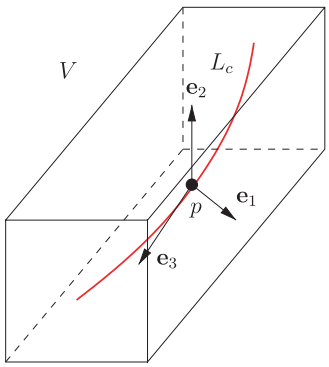

Figure 5. The three-dimensional computational domain for computation of stress intensity factors and interaction integrals.

The domain form of the interaction integral is then given by

$$I(p) = -\frac{\int_V (\mathrm{tr}(\mathbf{P}\cdot\nabla\mathbf{q}) + (\nabla\cdot\mathbf{P}^{\mathrm{T}})\cdot\mathbf{q})\,\mathrm{d}V}{\int_{L_c}\alpha_q(\mathbf{x})\,\mathrm{d}L_c} \tag{26}$$

assuming that the crack surfaces are traction-free [35]. Here, the tensor $\mathbf{P}$ is given by

$$\mathbf{P} = \boldsymbol{\sigma}:\boldsymbol{\varepsilon}^{\mathrm{aux}}\mathbf{I} - \nabla\mathbf{u}^{\mathrm{aux}}\cdot\boldsymbol{\sigma} - \nabla\mathbf{u}\cdot\boldsymbol{\sigma}^{\mathrm{aux}} \tag{27}$$

where fields with the superscript 'aux,' such as $\mathbf{u}^{\mathrm{aux}}$, denote auxiliary fields as in the previous section. The interaction integral $I(p)$ is locally path-independent, and related to the SIF components through the relation

$$I(p) = \frac{2}{E^*\cosh^2(\pi\varepsilon)}[K_1(p)K_1^{\mathrm{aux}} + K_2(p)K_2^{\mathrm{aux}}] + \frac{1}{\mu^*}K_3(p)K_3^{\mathrm{aux}} \tag{28}$$

where the effective shear modulus is given by

$$\mu^* = \frac{2\mu_1\mu_2}{\mu_1+\mu_2} \tag{29}$$

Thus, the SIF $K_1(p)$, $K_2(p)$ and $K_3(p)$ can then be computed with a proper choice of K_1^{aux}, K_2^{aux} and K_3^{aux}. For example, we can evaluate $K_1(p)$ by

$$K_1(p) = \frac{E^*\cosh^2(\pi\varepsilon)}{2} I(p, (K_1^{\mathrm{aux}}=1, K_2^{\mathrm{aux}}=0, K_3^{\mathrm{aux}}=0)) \tag{30}$$

3.3. Implementation

Next, we shall describe our implementation for the computation of the interaction integrals for both two and three dimensions. We first define our computational domain as a rectangular domain A (of size $L_1\times L_2$) around our crack tip in two dimensions or a rectangular parallelepiped domain V (of size $L_1\times L_2\times L_3$) around the point p on the crack front in three dimensions. We then subdivide the domain into several sub-domains (triangles in two dimensions and tetrahedra in three

DOI: 10.1002/nme

dimensions) so that the edges or faces of these sub-elements are aligned with the crack line or crack face. We then employ a higher-order Gauss integration scheme in each of these sub-domains to compute our interaction integral numerically.

In two dimensions, the function q is chosen to be a bilinear function that vanishes on the boundary of A and is unity at the crack tip

$$q(\hat{x}_1, \hat{x}_2) = \left(1 - 2\frac{|\hat{x}_1|}{L_1}\right)\left(1 - 2\frac{|\hat{x}_2|}{L_2}\right) \tag{31}$$

In three dimensions, the function $\alpha_q(\mathbf{x})$ is a trilinear function that vanishes on the boundary of V and is unity at p

$$\alpha_q(\hat{x}_1, \hat{x}_2, \hat{x}_3) = \left(1 - 2\frac{|\hat{x}_1|}{L_1}\right)\left(1 - 2\frac{|\hat{x}_2|}{L_2}\right)\left(1 - 2\frac{|\hat{x}_3|}{L_3}\right) \tag{32}$$

With the above choice of functions $\alpha_q(\mathbf{x})$, the denominator in (26) can be approximated by

$$\int_{L_c} \alpha_q(\mathbf{x})\, \mathrm{d}L_c \sim \frac{L_3}{2} \tag{33}$$

Here, $\hat{x}_1$, $\hat{x}_2$, $\hat{x}_3$ correspond to local coordinate components of the associated point in the vector basis $(\mathbf{e}_1, \mathbf{e}_2, \mathbf{e}_3)$.

4. NUMERICAL RESULTS

For simplicity, we shall use dimensionless quantities in this section. If not mentioned specifically, the smallest geometry parameter (such as the crack length), the smallest Young's modulus and tension magnitude are chosen to be unity.

4.1. A center crack in an infinite bimaterial plate

We consider an isolated crack of length $2a$ lying on the interface in a bimaterial solid subjected to the remote tension $\sigma_0^\infty + \mathrm{i}\tau_0^\infty$. The exact solution for the mixed-mode SIFs at the right crack tip is given by [37] as

$$K_1 + \mathrm{i}K_2 = (\sigma_0^\infty + \mathrm{i}\tau_0^\infty)(1 + 2\mathrm{i}\varepsilon)\sqrt{\pi a}(2a)^{-\mathrm{i}\varepsilon} \tag{34}$$

We only consider the case of pure tension loading. The plate is square with $H = W = 10$ as shown in Figure 6. We assume plane strain and choose $\nu_1 = \nu_2 = 0.3$. We expect to obtain good accuracy for small a/W. We consider three meshes:

- mesh 1: an unstructured mesh contains 18 767 elements with the interface arbitrarily aligned within the mesh.
- mesh 2: a structured mesh contains 127×127 elements with the interface passing through the elements as shown in Figure 7.
- mesh 3: a structured mesh contains 128×128 elements with the interface coincident with element edges.

We model the interface between the two materials, discontinuities across the crack and the crack tip field by the weak discontinuities (except in mesh 3), strong discontinuities and crack tip enrichments, respectively. We used 12 enrichments (16) for the crack tip enrichment. For the case

DOI: 10.1002/nme

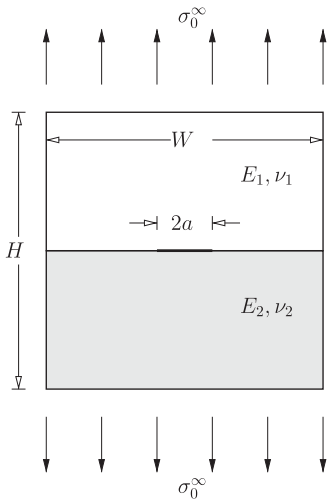

Figure 6. The bimaterial center crack.

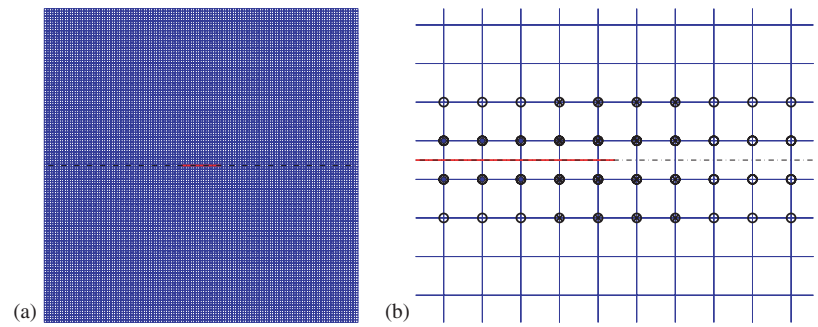

Figure 7. Center bimaterial crack mesh: (a) mesh 2 and (b) mesh near right crack tip: (○) abs-enrichment, (×) crack tip enrichment, (●) Heaviside enrichment.

$E_1/E_2 = 10$ and $a = 0.5$, we obtained almost identical SIF results with the three meshes as shown in Table I.

We present SIF results for several crack length parameters using mesh 2 in Figure 8. Excellent agreement with the exact solutions is observed. The average error is only 0.6% for K_1 and 0.9% for K_2. Our results are better than the earlier results in [25], thanks to the improved accuracy of the corrected XFEM. In [25], the same problem was solved using the same enrichment functions, but only half the crack is modeled. The authors employed mesh conforming with the material interface with a 400×400 mesh, and they obtained an accuracy of 1.1% for K_1 and 1.7% for K_2.

The same problem was also solved using only four enrichments (18). Again we obtain excellent accuracy: the maximum error is only 0.8% for K_1 and 1% for K_2, only slightly larger than our previous results. The reason is that in this particular case $\varepsilon = -0.0758$; hence, $\cos(\varepsilon \log r) \approx 1$, $\sin(\varepsilon \log r) \approx 0$, $e^{\varepsilon\theta} \approx e^{-\varepsilon\theta} \approx 1$ and the 12 bimaterial crack tip functions (16) can be well approximated by the regular four crack tip enrichments (18).

DOI: 10.1002/nme

Table I. The center crack: stress intensity factor results.

	Mesh 1	Mesh 2	Mesh 3	Analytical
K_1	1.2648	1.2525	1.2667	1.2533
K_2	−0.1924	−0.1888	−0.1920	−0.1900

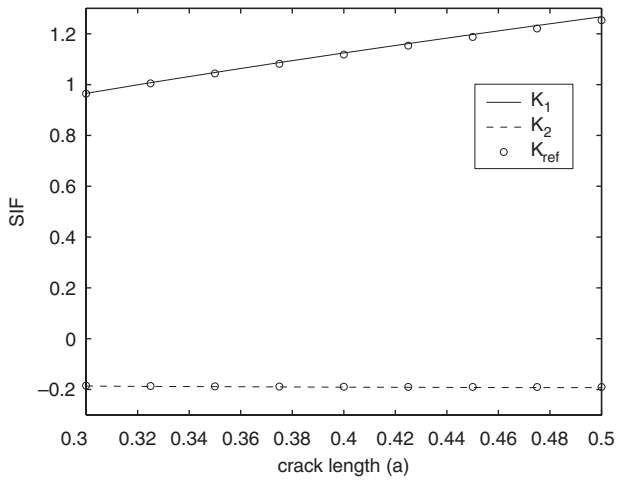

Figure 8. The bimaterial center crack stress intensity factors for $E_1/E_2 = 10$.

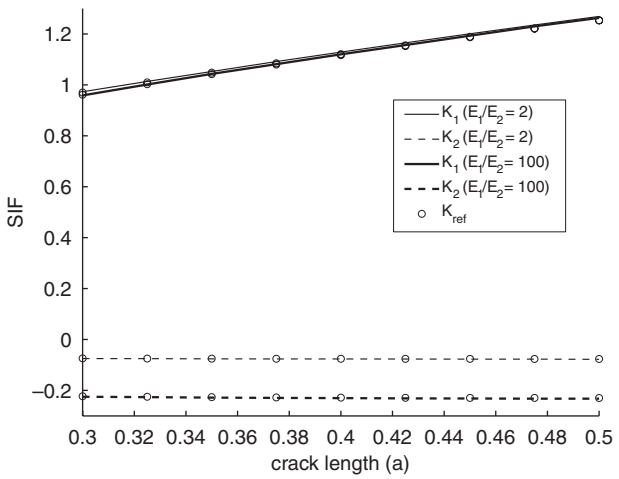

Figure 9. The bimaterial center crack stress intensity factors for $E_1/E_2 = 2, 100$.

We further demonstrate our results for the case $E_1/E_2 = 2$ and $E_1/E_2 = 100$, using four enrichments as the value ε for both cases are only of order 10^{-2}. Good accuracy is also observed as shown in Figure 9, even when the difference between the two material Young's moduli is fairly large.

DOI: 10.1002/nme

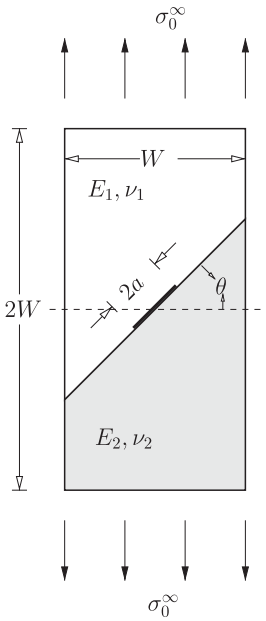

Figure 10. The slanted bimaterial crack.

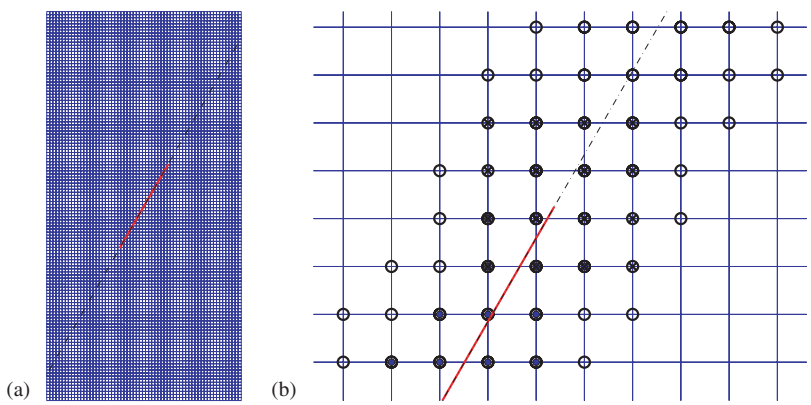

Figure 11. Slanted bimaterial crack mesh: (a) 64 × 128 mesh and (b) mesh near right crack tip: (○) abs-enrichment, (×) crack tip enrichment, (●) Heaviside enrichment.

We conclude that good accuracy can be obtained with the approximate four enrichment functions instead of the 12 enrichment functions. The advantages of using the four enrichment functions is obvious: the number of degrees of freedom is greatly reduced and the system is better conditioned. Furthermore, it is apparent that this high degree of accuracy can be obtained when the interface is modeled by an enrichment.

DOI: 10.1002/nme

4.2. A centered crack in a slanted bimaterial plate

We now consider the problem of center slanted crack in a finite bimaterial plate subjected to a uniaxial uniform tension σ_0. In the model shown in Figure 10, $a/W=0.5$ and $W=2$. The material properties are $E_1/E_2=10$ and $v_1=v_2=0.3$. This problem is solved in [38] using a boundary element method. Similar to the previous problem, we used a structured mesh and modeled the interface between the two materials, discontinuities across the crack and the crack tip field by the weak discontinuities, strong discontinuities and crack tip enrichments, respectively.

A 64×128 mesh and four enrichment functions are used as shown in Figure 11. We show our results in Figure 12. Good agreement between our method and the earlier results is obtained.

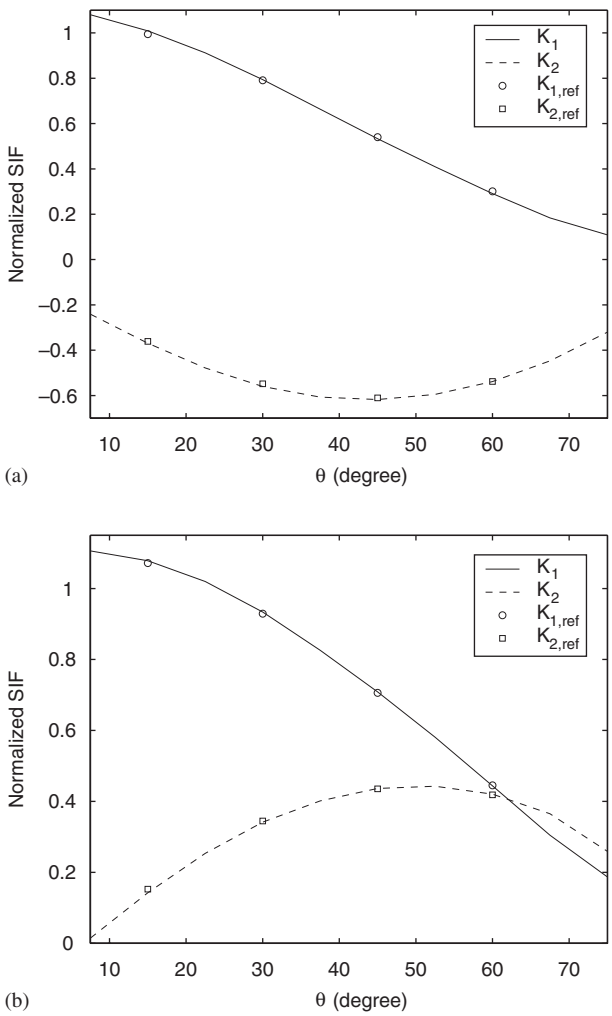

Figure 12. Slanted bimaterial crack: normalized stress intensity factors: (a) left crack tip and (b) right crack tip.

DOI: 10.1002/nme

4.3. Two-dimensional unit cell with cracks on fiber–matrix interface

We consider a two-dimensional unit cell that contains a circular fiber and two fiber–matrix interfacial cracks as shown in Figure 13 with the aim of examining the error due to using the straight interface enrichment for a curved interface. The unit cell is subjected to unit remote tension at both ends. The material properties are $E_1/E_2 = 10$ and $v_1 = v_2 = 0.3$. Owing to the symmetry of the problem, we only model a quarter as shown in Figure 13 and apply symmetric boundary conditions on the two faces corresponding to $x_1 = 0$ and $x_2 = 0$. The accuracy of the crack tip enrichments for curved cracks is studied in this example. We consider two types of mesh:

- unstr1, unstr2, unstr3, unstr4, unstr5 denote unstructured meshes with the interface and crack coincident with element edges and have characteristic element lengths of $\frac{1}{16}$, $\frac{1}{32}$, $\frac{1}{64}$, $\frac{1}{128}$ and $\frac{1}{256}$ at the vicinity of the crack tip, respectively.
- str1, str2, str3, str4 denote structured meshes with the interface passing through the elements and contain 15×15, 31×31, 63×63 and 127×127 elements, respectively.

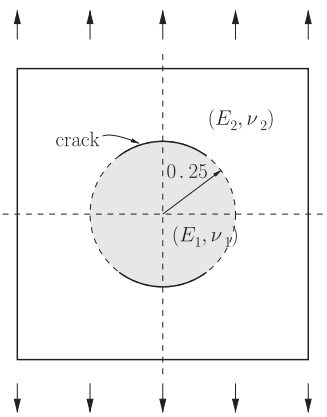

Figure 13. The two-dimensional unit cell for a matrix with one fiber.

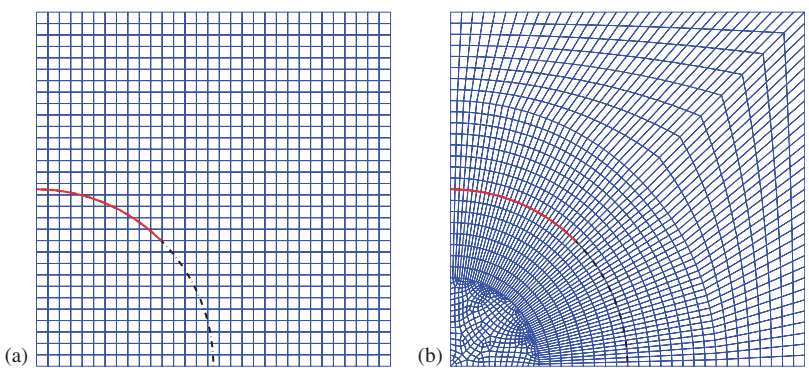

Figure 14. Two-dimensional fiber–matrix interfacial crack mesh: (a) unstr2 and (b) str2.

DOI: 10.1002/nme

Table II. The two-dimensional fiber–matrix interfacial crack: normalized stress intensity factor results for structured meshes (strI) and unstructured meshes (unstrI).

	str1	str2	str3	str4
K_1	1.0196	0.9933	0.9945	0.9926
K_2	1.0954	1.0046	0.9921	0.9927
	unstr1	unstr2	unstr3	unstr4
K_1	0.9653	0.9787	0.9921	0.9957
K_2	1.0175	0.9978	0.9957	0.9986

We show two meshes unstr2 and str2 in Figure 14. We model the interface between the two materials and discontinuities across the crack by the weak discontinuities, strong discontinuities for structured meshes, respectively; crack tip enrichments were used for all meshes. We used 12 enrichments (16) for the crack tip enrichment. Results are given in Table II; the results are normalized with the SIF result of mesh unstr5. The unstructured mesh results converge almost uniformly to the finest mesh (unstr5, 127×127 elements), which indicate that the approximations in the enrichment due to the absence of curvature do not impair convergence.

4.4. A penny-shaped crack in an infinite bimaterial solid

We consider the problem of a penny-shaped crack of radius a on the interface in a bimaterial solid subjected to remote tension σ_0^∞. The exact solution for the complex SIFs (K_1 and K_2) for any point on the crack front is given in [35] as

$$K_1 + \mathrm{i}K_2 = 2\sigma_0^\infty \sqrt{a} \frac{\Gamma(2+\mathrm{i}\varepsilon)}{\Gamma(\frac{1}{2}+\mathrm{i}\varepsilon)} (2a)^{-\mathrm{i}\varepsilon} \tag{35}$$

where Γ is the gamma function and ε is the bimaterial constant.

Owing to the symmetry of the problem, we only model a quarter as shown in Figure 15 and apply symmetric boundary conditions on the two faces corresponding to $x_1 = 0$ and $x_2 = 0$. Similar to our previous two-dimensional examples, we use a structured mesh and model the material interface, discontinuities across the crack and the crack tip field by the weak discontinuities, strong discontinuities and crack tip enrichments, respectively. The material properties are chosen to be $E_2/E_1 = 3$ and $\nu_1 = 0.22$, $\nu_2 = 0.3$, which are also used in [35]. The chosen material properties yield a small bimaterial constant, $\varepsilon = 0.0656$.

The structured mesh is of size $23 \times 23 \times 45$ as shown in Figure 16. Both (full) 13 crack tip enrichments and (approximate) four crack tip enrichments are used. The material interface is not coincident with element edges. In an earlier article, Gosz *et al*. [35] used a refined tetrahedral mesh around the crack front that consisted of 7257 nodes, in which the smallest element at the crack front has a characteristic length of $a/500$, and achieved an accuracy of 3% for K_1 and 2.63% for K_2.

We show our results in Table III for several crack radii and crack angles. Good agreements with the analytical results [37] are observed for both cases. The average SIF errors using 13 enrichment functions are about 1.00% for K_1 and 4.33% for K_2; and the average SIF errors with four enrichment functions are about 3.02% for K_1 and 6.48% for K_2. As expected, the use of 13

DOI: 10.1002/nme

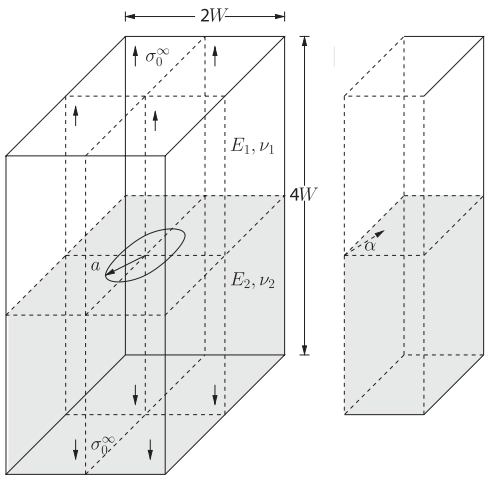

Figure 15. The penny-shaped bimaterial interface crack.

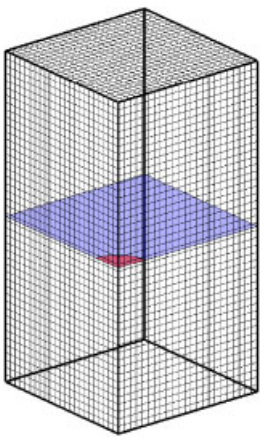

Figure 16. The penny-shaped crack mesh.

enrichment functions leads to better results; however, it is noted that good accuracy can also be obtained with the approximate four enrichment functions.

There are several advantages of using the approximate four enrichment functions. First, it leads to a model with fewer degrees of freedom, especially in the three-dimensional case. Second, the approximate four enrichment functions can also be used when the crack is not completely on the material interface; this may be advantageous for crack growth simulations.

4.5. Three-dimensional unit cell with a crack on fiber–matrix interface

We consider a fiber–matrix interfacial crack in a unit cell of a composite. The unit cell is subjected to remote tension at both ends and contains a cylindrical fiber with a crack lying on the matrix–fiber interface as shown in Figure 17. We denote the radius of the cylindrical fiber by a. The crack size

DOI: 10.1002/nme

Table III. The penny-shaped crack: stress intensity factor errors.

	$a/W=0.08$		$a/W=0.10$		$a/W=0.12$	
α	K_1 (%)	K_2 (%)	K_1 (%)	K_2 (%)	K_1 (%)	K_2 (%)
Thirteen enrichments						
$\pi/6$	1.99	6.59	1.06	3.36	0.78	4.81
$\pi/4$	0.48	4.28	0.59	4.86	0.64	4.70
$\pi/3$	1.93	5.07	1.08	3.46	0.44	1.88
Four enrichments						
$\pi/6$	3.54	8.07	3.16	6.52	2.77	6.06
$\pi/4$	3.38	6.81	2.59	4.10	2.05	4.91
$\pi/3$	3.71	6.47	3.40	7.79	2.55	7.62

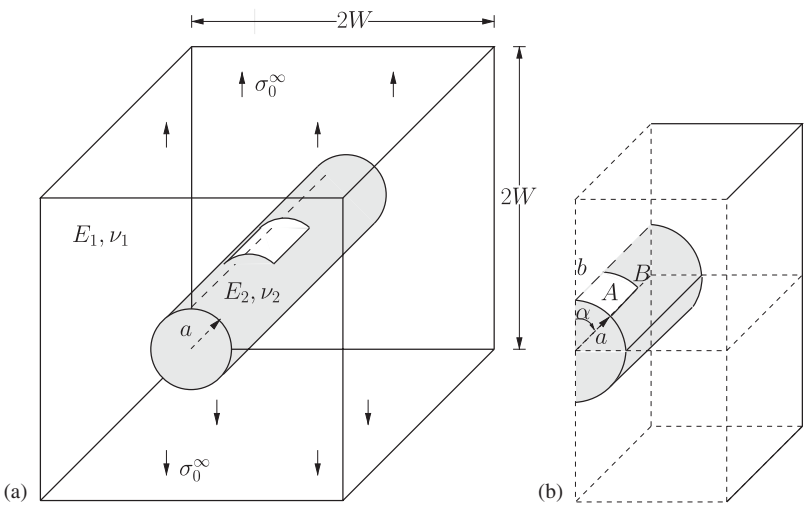

Figure 17. The three-dimensional unit cell for a matrix with one fiber.

is determined by the angle α and the crack length b as shown in Figure 17; we note that the crack faces are non-planar.

We choose the crack geometry parameters described above as $\alpha=\pi/4$ and $b=\pi a/4$, where $a/W=\frac{4}{15}$ and $W=10$. The parameters are chosen to represent a curved 'square'-shaped crack. Owing to the symmetry of the problem, we only model a quarter as shown in Figure 15 and apply symmetric boundary conditions on the two faces corresponding to $x_1=0$ and $x_2=0$. As in our previous two-dimensional examples, we used a structured mesh and model the interface between the two materials, discontinuities across the crack and the crack tip field by the weak discontinuities, strong discontinuities and crack tip enrichments, respectively. The material properties are chosen to be $E_2/E_1=100$ and $\nu_1=\nu_2=0.3$. These material properties yield a small bimaterial constant $\varepsilon=0.0916$.

DOI: 10.1002/nme

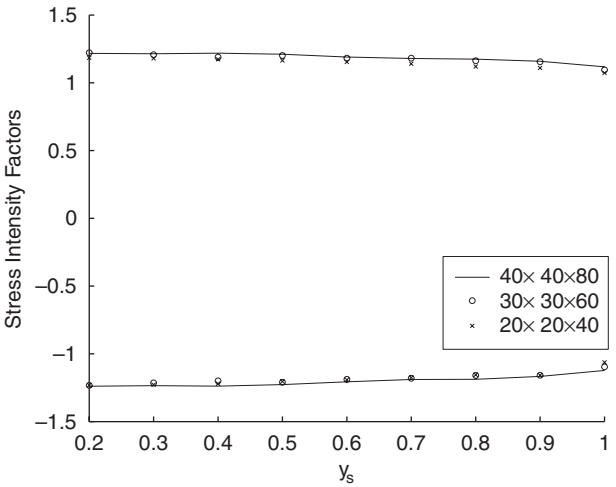

Figure 18. Stress intensity factors of the one fiber unit cell problems: K_1 (upper) and K_2 (lower).

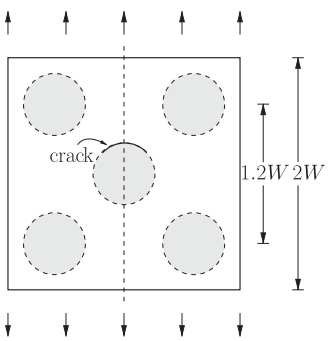

Figure 19. The three-dimensional unit cell for a matrix with five fibers.

We use a structured mesh and enrich the crack tip field by the (approximate) four crack tip functions. SIFs are calculated along the crack front, which is indicated by AB in Figure 17. We show results for $K_1(s)$ and $K_2(s)$ in Figure 18, here y_s is the distance between the point s and the point A. The result seems to be converged for a $40\times40\times80$ mesh, which corresponds to a system with 446 472 degrees of freedom.

We next considered the effect of multiple fibers on the composite structure strength. We consider five fibers in the unit cell: a cross section of the unit cell is shown in Figure 19.

The same structured mesh with $40\times40\times80$ elements is used; no mesh modification is required even with the changes in the morphology of the composites. The new system contains 489 816 degrees of freedom; here the additional $\sim$45 000 degrees of freedom are contributed by the enrichment nodes near the newly added fibers. SIFs along the edge AB are computed and compared with the previous results of the one-fiber composite model. The two results are plotted together in Figure 20, and show that the additional four fibers decrease the SIFs: the average K_1 and K_2 SIFs along the edge AB are about 7 and 14% smaller than before.

DOI: 10.1002/nme

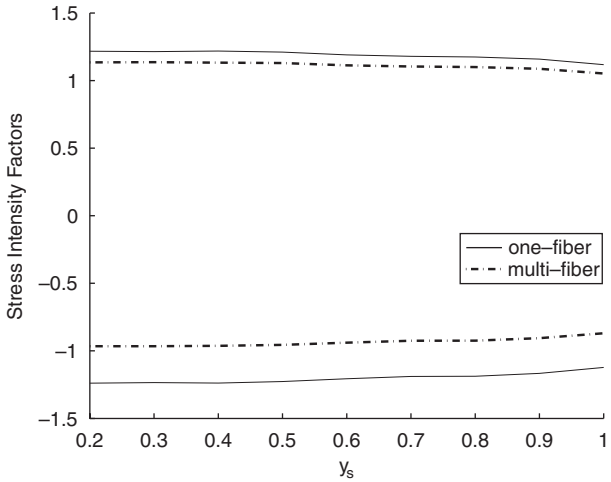

Figure 20. Stress intensity factor comparisons for one- and five-fiber unit cell problems: K_1 (upper) and K_2 (lower).

4.6. A multi-fiber composite model

Next, we consider a unit cell of a composite model with six fibers, each in different directions. In addition, the model contains 12 fiber–matrix interfacial cracks as shown in Figure 22. The example is chosen to demonstrate the versatility of our method, i.e. that no meshing of the interfaces or cracks is required and structured elements can be used. For traditional FEM, meshing such a model is very complex and time consuming.

We note that there is no intersection between two different fibers in the model. Let us denote r_α^{int} as the radius of the cylindrical fiber α. Assuming that the fiber is specified by a longitudinal unit-length vector $\hat{\mathbf{e}}_\alpha^{\text{int}}$ and a point $\mathbf{x}_{C,\alpha}^{\text{int}}$ on its axis, the level set function $f_\alpha^{\text{int}}(\mathbf{x})$ is given by

$$f_\alpha^{\text{int}}(\mathbf{x}) = \sqrt{(\mathbf{x}-\mathbf{x}_{C,\alpha}^{\text{int}})^{\mathrm{T}}(\mathbf{I}-\hat{\mathbf{e}}_\alpha^{\text{int}}(\hat{\mathbf{e}}_\alpha^{\text{int}})^{\mathrm{T}})(\mathbf{x}-\mathbf{x}_{C,\alpha}^{\text{int}})} - r_\alpha^{\text{int}} \tag{36}$$

All crack edges in the model are defined as intersections of two perpendicular cylinders of different radii. Thus, the level set function $g_\alpha^{\text{cr}}(\mathbf{x})$ for a crack α that lies on interface β is given by

$$g_\alpha^{\text{cr}}(\mathbf{x}) = r_\alpha^{\text{cr}} - \sqrt{(\mathbf{x}-\mathbf{x}_{C,\beta}^{\text{int}})^{\mathrm{T}}(\mathbf{I}-\hat{\mathbf{e}}_\alpha^{\text{cr}}(\hat{\mathbf{e}}_\alpha^{\text{cr}})^{\mathrm{T}})(\mathbf{x}-\mathbf{x}_{C,\beta}^{\text{int}})} \tag{37}$$

where r_α^{cr} is the radius of the crack and $\hat{\mathbf{e}}_\alpha^{\text{cr}} \cdot \hat{\mathbf{e}}_\beta^{\text{int}} = 0$. The crack front is given by $f_\beta^{\text{int}}(\mathbf{x}) = g_\alpha^{\text{cr}}(\mathbf{x}) = 0$.

The solid is subjected to unit tension on all six sides. A structured $40 \times 40 \times 40$ mesh is used. We show the mesh and the effective stress in Figure 21, and the displacement field in a specified plane in Figure 22. To display the discontinuities, elements containing enrichments in the slice

DOI: 10.1002/nme

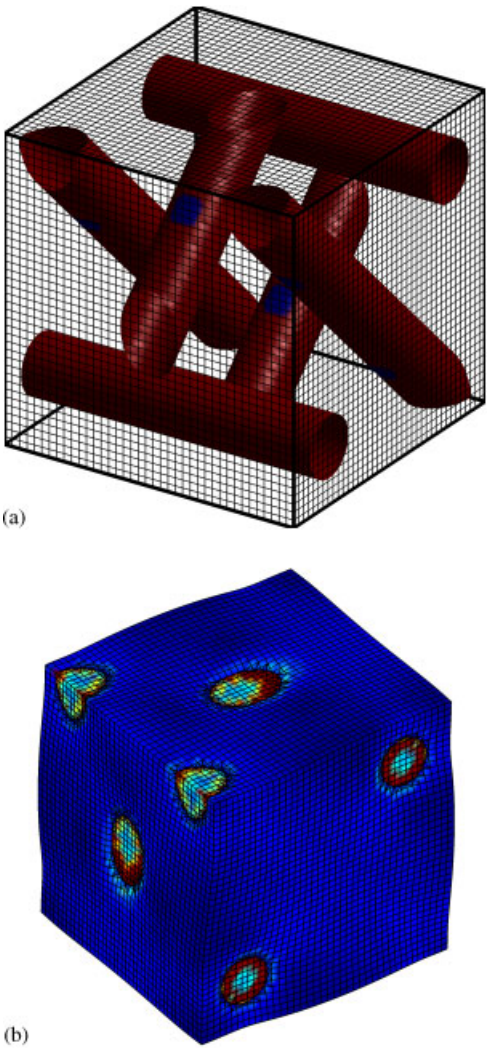

Figure 21. A unit cell of the multi-fiber composite: (a) 40 × 40 × 40 mesh and (b) von-Mises stress.

are decomposed into tetrahedra and displacement values are corrected in each tetrahedron. Four interfacial crack openings along the fiber are clearly visible in the figure.

5. CONCLUSION

In this article, we described further developments in XFEM for crack problems in composite materials and solids with interfaces. These methods do not impose any restriction on the computational mesh. Both strong discontinuities across the crack and weak discontinuities across the material interface are modeled by XFEM. The accuracy is further enhanced by using a blending-corrected

DOI: 10.1002/nme

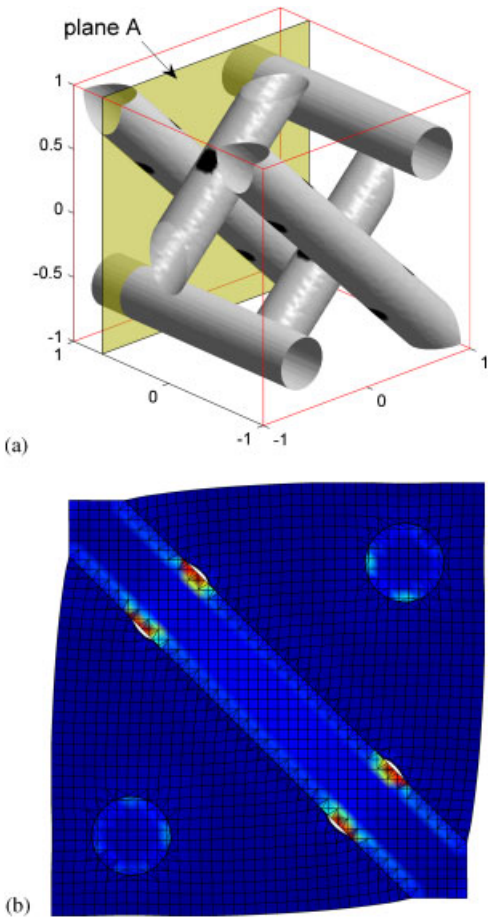

Figure 22. A unit cell of the multi-fiber composite: (a) the depiction of cracks and plane A and (b) displacement field in plane A.

XFEM that improves the approximation in blending elements described in [23, 24]. We show several numerical examples to demonstrate the accuracy and versatility of the method. Results with full and approximate enrichments for the bimaterial crack tips were obtained. Full enrichments give better results; however, good accuracy can also be achieved using the approximate enrichments with less complexity and computational cost.

Although the example shown here employed structured meshes, arbitrary meshes can be used. The examples given here were unit cells, where structured meshes are more convenient. However, arbitrary complex structures can be modeled by the same methodology.

A key finding of the numerical studies is that the weak discontinuity enrichment suffices for modeling the interface for cracks at interfaces. Comparison of results with previous benchmarks shows that such models provide high accuracy. The modeling of the interface by weak discontinuity enrichments provides a terrific advantage since it simplifies meshing.

This methodology offers great potential in the study of composite failure and the engineering of composites. Other failure laws, such as cohesive laws, can easily be added in XFEM (see,

DOI: 10.1002/nme

e.g. Moës and Belytschko [9]) and the methodology can be extended to anisotropic materials. Furthermore, the method can readily be extended to evolving cracks or cracks not on the interfaces, by methods such as those described in Stolarska *et al*. [32] and Gravouil *et al*. [10].

APPENDIX A

The following gives the near-tip displacement fields for a crack at a bimaterial interface between two isotropic materials. The solution and auxiliary displacement field are defined in the local coordinate system defined by $(\mathbf{e}_1, \mathbf{e}_2, \mathbf{e}_3)$ as shown in Figure 5. They are given by

$$u_1^{\text{aux}}(r,\theta) = \frac{1}{4\mu_i \cosh(\pi\varepsilon)}\sqrt{\frac{r}{2\pi}}(f_{11}K_1 + f_{12}K_2 + f_{13}K_3) \tag{A1}$$

$$u_2^{\text{aux}}(r,\theta) = \frac{1}{4\mu_i \cosh(\pi\varepsilon)}\sqrt{\frac{r}{2\pi}}(f_{21}K_1 + f_{22}K_2 + f_{23}K_3) \tag{A2}$$

$$u_3^{\text{aux}}(r,\theta) = \frac{2}{\mu_i}\sqrt{\frac{r}{2\pi}}(f_{31}K_1 + f_{32}K_2 + f_{33}K_3) \tag{A3}$$

where $\mu_i, i = 1\ldots2$, correspond to the shear modulus of materials 1 and 2, respectively; r and θ correspond to a local polar coordinate system defined by the geometry at the crack tip as shown in Figure 4. The material constant ε is defined by

$$\varepsilon = \frac{\mu_1 + \mu_2\kappa_1}{\mu_2 + \mu_1\kappa_2} \tag{A4}$$

where κ_i is the Kolosov constant related to the Poisson ratio by $\kappa_i = 3 - 4\nu_i$ in plane strain. The terms $f_{ij}, i, j = 1\ldots3$ are given by

$$f_{11} = D_i + 2\delta_i \sin\theta \sin\phi \tag{A5}$$

$$f_{12} = -C_i + 2\delta_i \sin\theta \cos\phi \tag{A6}$$

$$f_{21} = -C_i - 2\delta_i \sin\theta \cos\phi \tag{A7}$$

$$f_{22} = -D_i + 2\delta_i \sin\theta \sin\phi \tag{A8}$$

$$f_{33} = \sin\frac{\theta}{2} \tag{A9}$$

$$f_{13} = f_{23} = f_{31} = f_{32} = 0 \tag{A10}$$

where C, D and δ_i are given by

$$\delta_1 = \mathrm{e}^{-\pi+\theta\varepsilon} \tag{A11}$$

$$\delta_2 = \mathrm{e}^{\pi+\theta\varepsilon} \tag{A12}$$

$$\phi = \varepsilon \ln(r) + \frac{\theta}{2} \tag{A13}$$

DOI: 10.1002/nme

$$C_i = \overline{\beta}\gamma_i \cos\frac{\theta}{2} - \beta\overline{\gamma}_i \sin\frac{\theta}{2} \tag{A14}$$

$$D_i = \beta\gamma_i \cos\frac{\theta}{2} + \overline{\beta}\overline{\gamma}_i \sin\frac{\theta}{2} \tag{A15}$$

$$\beta = \frac{2\cos(\varepsilon\ln(r)) + 4\varepsilon\sin(\varepsilon\ln(r)))}{1+4\varepsilon^2} \tag{A16}$$

$$\overline{\beta} = \frac{2\cos(\varepsilon\ln(r)) - 4\varepsilon\sin(\varepsilon\ln(r)))}{1+4\varepsilon^2} \tag{A17}$$

$$\gamma_i = \kappa_i\delta_i - \frac{1}{\delta_i} \tag{A18}$$

$$\overline{\gamma}_i = \kappa_i\delta_i + \frac{1}{\delta_i} \tag{A19}$$

The auxiliary strain and stress fields are obtained from the auxiliary displacement fields using Hooke's law.

REFERENCES

1. Black T, Belytschko T. Elastic crack growth in finite elements with minimal remeshing. *International Journal for Numerical Methods in Engineering* 1999; **45**:601–620.
2. Daux C, Moës N, Dolbow J, Sukumar N, Belytschko T. A finite element method for crack growth without remeshing. *International Journal for Numerical Methods in Engineering* 1999; **46**:131–150.
3. Babuska I, Melenk JM. The partition of unity method. *International Journal for Numerical Methods in Engineering* 1997; **40**(4):727–758.
4. Duarte CA, Reno LG, Simone A. A generalized finite element method for polycrystals with discontinuous grain boundaries. *International Journal for Numerical Methods in Engineering* 2006; **67**:1122–1145.
5. Duarte CA, Reno LG, Simone A. High-order generalized FEM for though-the-thickness branched cracks. *International Journal for Numerical Methods in Engineering* 2007; **72**:325–351.
6. Belytschko T, Moës T, Usui S, Parimi C. Arbitrary discontinuities in finite elements. *International Journal for Numerical Methods in Engineering* 2001; **50**:993–1013.
7. Belytschko T, Black T. Elastic crack growth in finite elements with minimal remeshing. *International Journal for Numerical Methods in Engineering* 1999; **45**:601–620.
8. Bordas S, Nguyen PV, Durant C. An extended finite element library. *International Journal for Numerical Methods in Engineering* 2007; **71**:703–732.
9. Moës N, Dolbow J, Belytschko T. A finite element method for crack growth without remeshing. *International Journal for Numerical Methods in Engineering* 1999; **46**:131–150.
10. Gravouil A, Moës N, Belytschko T. Non-planar 3d crack growth by the extended finite element and level sets—part ii: level set update. *International Journal for Numerical Methods in Engineering* 2002; **53**:2569–2586.
11. Moës N, Gravouil A, Belytschko T. Non-planar 3d crack growth by the extended finite element and level sets—part i: mechanical model. *International Journal for Numerical Methods in Engineering* 2002; **53**:2549–2568.
12. Sukumar N, Moës N, Moran B, Belytschko T. Extended finite element method for three-dimensional crack modelling. *International Journal for Numerical Methods in Engineering* 2000; **48**:1549–1570.
13. Belytschko T, Chen H, Xu JX, Zi G. Dynamic crack propagation based on loss of hyperbolicity and a new discontinuous enrichment. *International Journal for Numerical Methods in Engineering* 2003; **58**:1873–1905.
14. Song J-H, Areias P, Belytschko T. A method for dynamic crack and shear band propagation with phantom nodes. *International Journal for Numerical Methods in Engineering* 2006; **67**:868–893.
15. Gracie R, Ventura G, Belytschko T. A new fast method for dislocations based on interior discontinuities. *International Journal for Numerical Methods in Engineering* 2007; **69**:1151–1173.

DOI: 10.1002/nme

16. Belytschko T, Gracie R. On XFEM applications to dislocations and interfaces. *International Journal of Plasticity* 2007; **23**:1721–1738.
17. Legrain G, Moës N, Verron E. Stress analysis around crack tips in finite strain problems using the extended finite element method. *International Journal for Numerical Methods in Engineering* 2005; **63**:290–314.
18. Fish J. The s-version of the finite-element method. *Computers and Structures* 1992; **43**:539–547.
19. Fish J, Markolefas S. The s-version of the finite-element method for multiplayer laminates. *International Journal for Numerical Methods in Engineering* 1992; **33**:1081–1105.
20. Fan R, Fish J. The RS-method for material failure simulations. *International Journal for Numerical Methods in Engineering* 2007; **73**:1607–1623.
21. Chessa J, Wang H, Belytschko T. On the construction of blending elements for the local partition of unity enriched finite elements. *International Journal for Numerical Methods in Engineering* 2003; **57**:1015–1038.
22. Béchet E, Minnebo H, Moës N, Burgardt B. Improved implementation and robustness study of the X-FEM for stress analysis around cracks. *International Journal for Numerical Methods in Engineering* 2005; **64**(8): 1033–1056.
23. Gracie R, Wang H, Belytschko T. Blending in the extended finite element method by discontinuous Galerkin and assumed strain methods. *International Journal for Numerical Methods in Engineering* 2008; DOI: 10.1002/nme.2217.
24. Fries TP. A corrected XFEM approximation without problems in blending elements. *International Journal for Numerical Methods in Engineering* 2007; DOI: 10.1002/nme.2259.
25. Sukumar N, Huang ZY, Prevóst JH, Suo Z. Partition of unity enrichment for bimaterial interface cracks. *International Journal for Numerical Methods in Engineering* 2004; **59**:1075–1102.
26. Liu XY, Xiao QZ, Karihaloo BL. XFEM for direct evaluation of mixed mode SIFS in homogeneous and bi-materials. *International Journal for Numerical Methods in Engineering* 2004; **59**:1103–1118.
27. Nagashima T, Omoto Y, Tani S. Stress intensity factor analysis of interface cracks using X-FEM. *International Journal for Numerical Methods in Engineering* 2003; **56**:1151–1173.
28. Hettich T, Ramm E. Interface material failure modeled by the extended finite-element method and level sets. *Computer Methods in Applied Mechanics and Engineering* 2005; **195**:4753–4767.
29. Yau J, Wang S, Corten H. A mixed-mode crack analysis of isotropic solids using conservation laws of elasticity. *Journal of Applied Mechanics* 1980; **47**:335–341.
30. Belytschko T, Parimi C, Moës N, Sukumar N, Usui S. Structured extended finite element methods for solids defined by implicit surfaces. *International Journal for Numerical Methods in Engineering* 2002; **56**:609–635.
31. Sukumar N, Chopp DL, Moës N, Belytschko T. Modeling holes and inclusions by level sets in the extended finite element method. *Computer Methods in Applied Mechanics and Engineering* 2000; **190**:6183–6200.
32. Stolarska M, Chopp DL, Moës N, Belytschko T. Modelling crack growth by level sets in the extended finite element method. *International Journal for Numerical Methods in Engineering* 2001; **51**:943–960.
33. Duflot M. A study of the representation of cracks with level-sets. *International Journal for Numerical Methods in Engineering* 2007; **70**:1261–1302.
34. Flemming M, Chu YA, Moran B, Belytschko T. Enriched element-free Galerkin methods for crack tip fields. *International Journal for Numerical Methods in Engineering* 1997; **40**:1483–1504.
35. Gosz M, Dolbow J, Moran B. Domain integral formulation for stress intensity factor computation along curved three-dimensional cracks. *International Journal of Solids and Structures* 1998; **35**(15):1763–1783.
36. Smelser SE. On the j-integral for bi-material bodies. *International Journal of Fracture* 1977; **13**:382–384.
37. Hutchinson JW, Suo Z. Mixed mode cracking in layered materials. In *Advances in Applied Mechanics*, vol. 29, Hutchinson JW, Wu TY (eds). Academic Press: San Diego, CA, 1991; 63–191.
38. Miyazaki M, Ikeda T, Soda T, Munakata T. Stress intensity factor analysis of interface crack using boundary element method—application of contour-integral method. *Engineering Fracture Mechanics* 1993; **45**(5):599–610.